RSC Advances

PAPER

View Article Online
View Journal | View Issue

Cite this: *RSC Adv.*, 2017, **7**, 9160

Structural, optical and magnetic properties of N ion implanted CeO_2 thin films

Pawan Kumar,[a] Parmod Kumar,[b] Ashish Kumar,[b] Indra Sulania,[b] F. Chand*[a] and K. Asokan*[b]

The present study reports the structural, morphological, optical and magnetic properties of N ion implanted CeO_2 thin films deposited by RF magnetron sputtering technique. These CeO_2 thin films were implanted with N ions having an energy of 80 keV with varying fluencies of 1×10^{15}, 1×10^{16} and 6×10^{16} ions per cm^2, respectively. X-ray diffraction measurements show that as deposited films had predominantly (111) orientations. There is a significant change in the crystalline nature of these films after implantation compared to pristine film. RBS measurements confirm the presence of N ions in CeO_2 thin film with the highest fluence. The closely packed circular shaped nanoparticles were observed through AFM images both in pristine and N ion implanted CeO_2 films and these were agglomerated on the surface at a fluence of 6×10^{16} ions per cm^2. The crystalline structure and defect related information were evident through Raman spectroscopy. Raman results show that the crystalline structure is maintained even after implantation while the defect related peak is highest for the fluence value of 1×10^{15} ions per cm^2 and decreases thereafter. The magnetic measurements show enhanced ferromagnetic ordering in N ion implanted CeO_2 films compared to pristine film. The saturation magnetization is highest for the lowest fluence of N ions (1×10^{15} ions per cm^2) which decreases with ion fluences. This diverse defect nature of oxygen vacancies (V_O) in the N ion implanted CeO_2 thin films mediates the ferromagnetic ordering.

Received 3rd July 2016
Accepted 23rd January 2017

DOI: 10.1039/c6ra17069b

rsc.li/rsc-advances

1. Introduction

CeO_2 is an important insulator that has been used in a wide variety of applications such as an epitaxial growth of buffer layers for high temperature superconducting thin films, high-*k* dielectric material in capacitors, solid oxide fuel cells, and as high oxygen storage devices.[1,2] This has also been extensively studied for efficient redox activities.[3] The discovery of room temperature ferromagnetism (RTFM) in various oxides doped with non-magnetic impurities has opened up a new direction in the field of spintronics. Due to the novel material properties and wide functionality, CeO_2 has been emerging as a superior oxide among the other rare earth oxides and as a potential candidate for spintronics applications.[4,5] The doping of transition metals like Mn, and Cu result in enhancement of ferromagnetism (FM) in CeO_2 nanocrystals.[6,7] The FM in diluted magnetic oxides (DMO) presents a major challenge in understanding its origin in such materials based on the general perception of exchange mechanisms. Dietl *et al.* proposed that the FM in DMO is not similar to the FM in group III–IV compounds like GaAs doped with Mn. The Zener model of the hole mediated mechanism is one of the possible explanations to understand such FM interactions.[8] The exact origin behind FM in DMO is still a matter of discussion. However, the defects such as oxygen vacancies (V_O), and the electronic configuration in lattice are known to play a major role in the FM.[9] Ge *et al.* proposed that the FM is strongly correlated in the presence of V_O.[10] A report by Coey *et al.* suggested that the FM in DMO can been explained using F-center exchange mechanism which is based on trapping of electrons in V_O (F-center) acting as coupling mediator between magnetic ions.[11] However, Liu *et al.* showed that the origin of RTFM in CeO_2 nanostructures is mediated by Ce vacancies rather than V_O.[12] Ranjith *et al.* proposed that surface O defect states attribute exchange interaction between unpaired spins which ultimately governs the FM in CeO_2 nanoparticles.[13] Cruz *et al.* reported the magnetic properties of Ar and N ion implanted TiO_2 rutile single crystals wherein the observed FM has been associated with different types of defects.[14] Recently, RTFM has been reported in C ion implanted ZnO thin films.[15] In case of C ion doped ZnO, the experimental and theoretical calculations suggest that the substitution of O by C ions results in production of V_O which results in ferromagnetic behaviour.[16] Elfimov *et al.* proposed that substitution of O with N ion leads to ferromagnetic behaviour in insulating oxides.[17] RTFM has also been observed in various non-TM doped metallic oxides such as Er doped ZnO, C-doped ZnO, and N-doped MgO.[18–20] Liu *et al.* reported spin polarized states as most stable when N ion

[a]*Department of Physics, Kurukshetra University, Kurukshetra, Haryana-136119, India. E-mail: fchand@kuk.ac.in*

[b]*Materials Science Division, Inter University Accelerator Centre, New Delhi-110067, India. E-mail: asokaniuac@gmail.com*

replaces O in MgO.[21] Kapilashrami *et al.* proposed that magnetization in N-doped MgO is strongly correlated with the formation of defects.[22] A report by Ben *et al.* suggested that FM in MgO nanosheets is attributable to unpaired electrons trapped at V_O.[23] Ion implantation is an efficient technique for doping the small concentration of ions and it has been employed to introduce FM into metal oxides.[24,25] The dopant concentration can be precisely controlled in a selected area which is a unique advantage of this technique. However, a large numbers of defects are introduced in materials as a result of ion implantation. These defects will certainly influence the ferromagnetic properties of implanted samples. As N ion has an ionic radius comparable to O and it is most suitable dopant.[26] The substitution of N at O sites implies creation of different kinds of defects which are in turn responsible for significant modification in various physical properties. Even though there are many reports on the RTFM in CeO_2, there are no reports about the effects of N ion implantation on the structural, optical, and magnetic properties. These magnetic films have potential applications in data storage devices, magnetic strips, actuators, magnetic sensors and microwave devices *etc.*[27,28]

Considering the importance of these materials, present study focuses on the detailed understanding of structural, morphological, optical and magnetic properties of N ion implanted CeO_2 thin films deposited by RF sputtering. This also provides an opportunity to understand the role of defects such as V_O and to establish the RTFM in CeO_2 system.

2. Experimental details

CeO_2 thin films were deposited on Si (111) substrates using RF magnetron sputtering. Before deposition, these substrates were cleaned by acetone and trichloroethylene. The chamber vacuum was better than 2×10^{-5} torr which is normally required for depositing high quality films. The deposition was carried out in Ar gas environment at RF power of 150 W for 1 hour at room temperature (*i.e.* without substrate heating). These CeO_2 films were then implanted with 80 keV of N^+ ion beam with a beam current of 2 μA using low energy ion beam facility (LEIBF) at Inter University Accelerator Centre (IUAC), New Delhi. The implantation was performed at three ion fluences; 1×10^{15}, 1×10^{16} and 6×10^{16} ions per cm^2. These N ion fluencies correspond to the total at% of N ions in CeO_2 films ~0.14, 1.4 and 8.4 respectively. These were estimated using TRIM simulation and confirmed by RBS measurements and XRUMP simulation. Hereafter these films are referred as: P (pristine CeO_2 film), N_{1E15} (CeO_2 N-ion implanted with fluence of (1×10^{15} ions per cm^2), N_{1E16} (1×10^{16} ions per cm^2) and N_{6E16} (6×10^{16} ions per cm^2). X-ray diffraction measurements were performed using X-ray diffractometer (Bruker D8) with CuKα radiation ($\lambda = 1.54$ Å) in order to obtain structural information within 20–60° range with step size of 0.02°. The Rutherford backscattering (RBS) measurements were performed with 2 MeV H^+ ions at IUAC, New Delhi. The incident and scattering angles were maintained at 7° and 170° respectively. The surface morphology of pristine and N ion implanted films was examined by a Multi Mode Scanning Probe Microscopy with Nanoscope IIIa controller from Digital/Veeco Instruments Inc. in tapping mode using RTESP tip with a tip radius of ~10 nm. The Raman spectra were recorded by using Renishaw InVia Raman microscope using wavelength ($\lambda = 514$ nm). The UV-VIS reflectance spectra were obtained using UV-vis Spectrophotometer (Model 2550). The photoluminescence (PL) spectra were carried out using the Spectrofluorometer (Shimadzu RF-5301PC). Furthermore, the magnetic properties were studied using vibrating sample magnetometer (VSM) (MicroSense EZ9 VSM).

3. Results and discussion

3.1 X-ray diffraction

To study the effect of N ion implantation on the structural parameters such as lattice parameter, strain and crystallite size in CeO_2 thin films, XRD measurements were carried out at room temperature. The XRD pattern of P and N ion implanted films are shown in Fig. 1. The sharp peaks are observed at the diffraction planes (111), (200), (220) and (311). These peaks match well with JCPDS card no. 75-0390 corresponding to the FCC fluorite structure of CeO_2 lattice. The intensity of prominent peak at 28.38° *i.e.*, (111) plane of N ion implanted films is significant and FWHM decreases with increasing ion fluences compared to the P film. The increasing intensity in XRD peak signifies an improvement in crystalline nature of CeO_2 films with N ion implantation. The average crystallite size of the CeO_2 is estimated from most prominent peak corresponding to (111) reflection plane using the Scherrer's formula[29] and listed in Table 1,

$$D = \frac{0.9\lambda}{\beta \cos \theta} \quad (1)$$

where D is the crystallite size, λ (1.54 Å) is wavelength of X-ray, β is FWHM and θ is Bragg's diffraction angle. The calculated data is shown in Table 1. The dislocation density 'δ' which is total length of dislocation lines per unit volume is measured

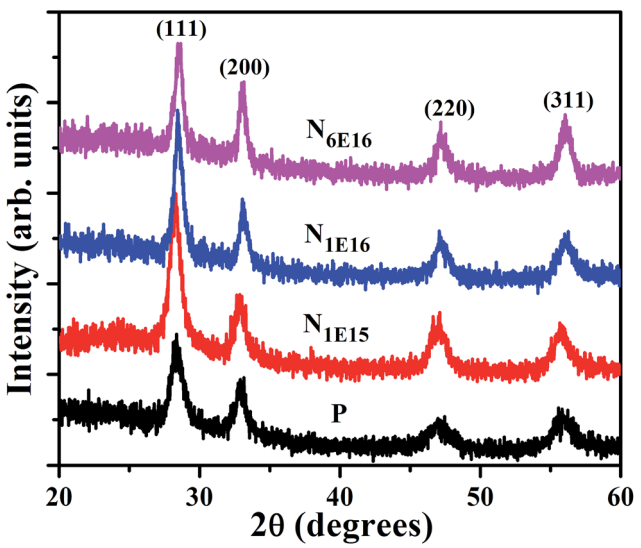

Fig. 1 XRD patterns of P and N ion implanted CeO_2 thin films.

Table 1 Structural and morphological parameters of P and N ion implanted CeO_2 thin films. The crystallite size, lattice parameter, strain and dislocation density were obtained from XRD while roughness and particle size from AFM

Ion fluence (ions per cm^2)	Crystallite size (nm)	Lattice parameter (Å)	Strain (ε) $\times 10^{-2}$	Roughness (nm)	Dislocation density, $\delta \times 10^{12}$ (m^{-2})	Particle size (nm)
P	8.0	5.441	7.11	3.20	1.547	59.4
N_{1E15}	8.7	5.462	6.41	2.62	1.327	60.2
N_{1E16}	10.8	5.421	6.34	2.61	0.853	61.3
N_{6E16}	11.8	5.417	3.15	2.56	0.718	81.7

using $\delta = 1/D^2$.[30] The dislocation density is found to decrease with ion fluences as given in Table 1. This decrease in the dislocation density corresponds to reduction of the disorder with increasing N ion fluence inside CeO_2 films. Furthermore, the lattice parameter of CeO_2 thin films is measured using the following expression,[31]

$$a^2 = \left[\frac{\lambda^2}{4\sin^2\theta}\right](h^2 + k^2 + l^2) \quad (2)$$

where a is lattice constant for FCC structure of CeO_2. The lattice parameter of P film (5.441 Å) is found larger than the bulk CeO_2, (5.411 Å) (JCPDS card no. 75-0390). It is also observed that lattice parameter of N_{1E15} film is higher compared to N_{1E16} and N_{6E16} films. This suggests that at lower concentration of N ions, these are likely to occupy O sites. It may be noted that the ionic radius of N (1.71 Å) ion is slightly larger than that of O (1.40 Å). Hence, this is likely to change in lattice parameter and create lattice strain which in turn affects various physical properties of CeO_2 thin films. The strain 'ε' is estimated using Williamson–Hall (W–H) analysis,[32] as shown in Fig. 2. The graphs were plotted between 4 sin(θ) (x-axis) and β cos(θ)/λ (y-axis). The slope of the linear fitted data corresponds to strain in the sample and listed in Table 1. The strain is found to be maximum for the P film and reduces with N ion fluence in the films. This indicates strain relaxation in the films after N ion implantation. The positive value of strain 'ε' corresponds to tensile strain in CeO_2 thin films.

3.2 Rutherford backscattering (RBS) spectrometry

In order to confirm the composition and thickness of the deposited films, RBS measurement was performed and then simulated with XRUMP software (Fig. 3). The simulated spectra show that the average thickness of the films are ~300 to 320 nm and the Ce : O ratio is 1 : 2. It is evident from Fig. 3 that N is detected for the highest fluence film (N_{6E16}). However, for lower fluences (N_{1E15} and N_{1E16}) implanted films, the signal from N in RBS was very weak because of low concentrations. Further, to confirm the depth and the distribution of N ions in CeO_2 thin films the TRIM calculations were carried out using SRIM software. From the Fig. 4, the depth of N ions in CeO_2 thin films is found to be ~110 nm and the distribution is Gaussian in nature. The observed depth of N ions inside CeO_2 thin film is consistent with the simulation of the RBS data using XRUMP software.

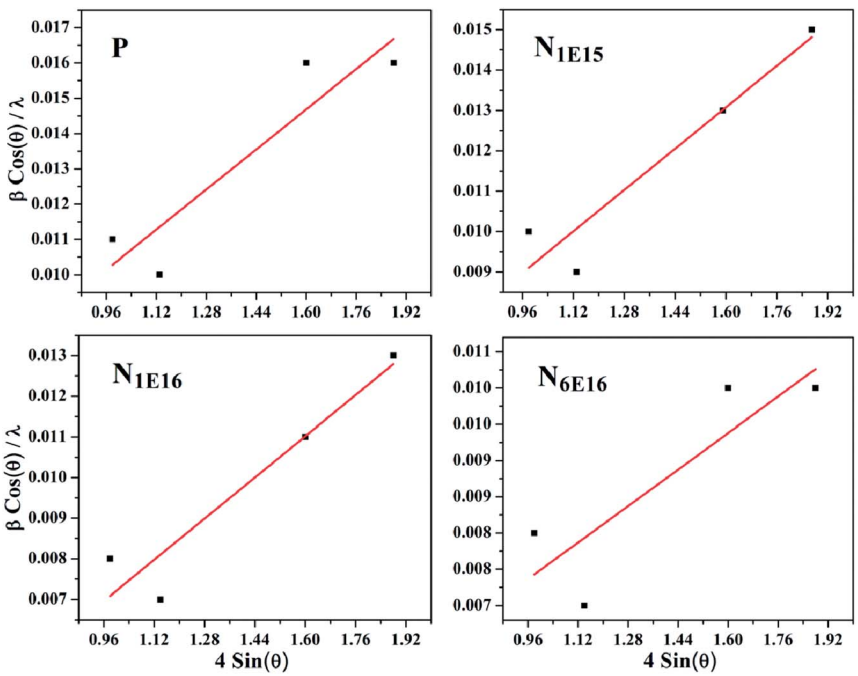

Fig. 2 W–H plot of P and N ion implanted CeO_2 thin films.

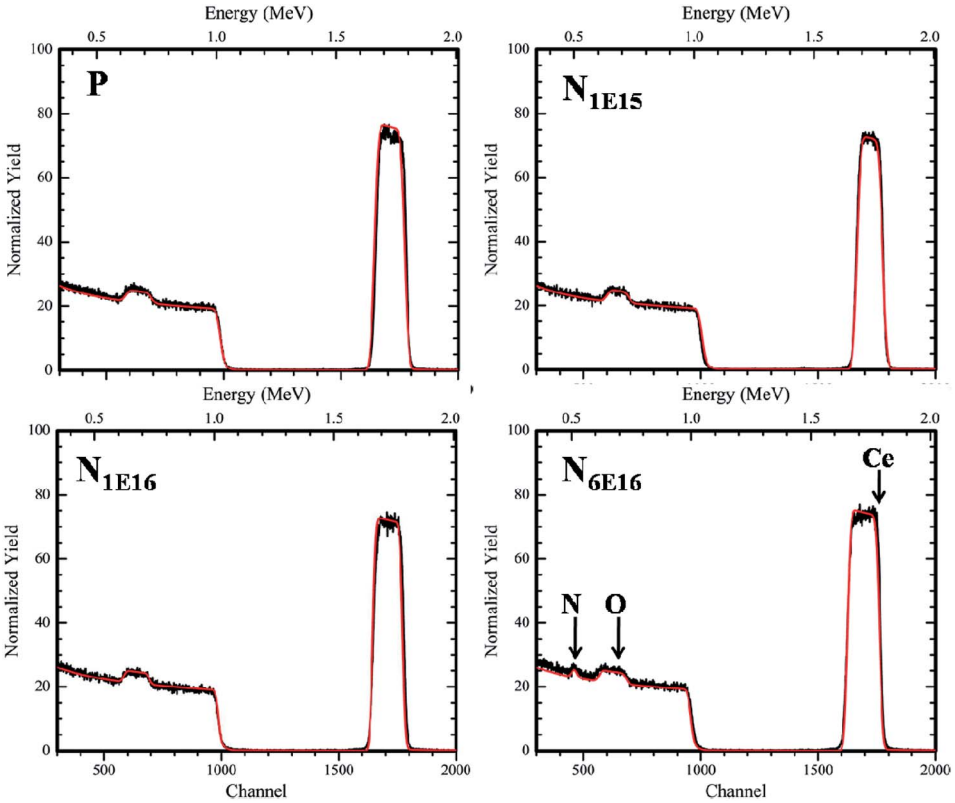

Fig. 3 Simulated RBS spectra of P and N ion implanted CeO_2 thin films.

3.3 Atomic Force Microscopy (AFM)

Fig. 5 shows AFM images of P and N ion implanted CeO_2 films. The formation of closely packed circular shaped nanoparticles on the surface of the films is clearly observed. It is evident that nanoparticles are well grown on the surface of the films and are uniformly distributed on 2 × 2 μm^2 scan area of the films. However, the surface morphology of N_{6E16} is slightly different from the P, N_{1E15} and N_{1E16} films indicating the effect of higher energy deposition at higher fluence of N ions. The smaller particles are agglomerated on the surface of N_{6E16} film. The average particle size and root mean square (RMS) surface roughness values of P, N_{1E15}, N_{1E16} and N_{6E16} films are given in Table 1. It is observed that the surface roughness decreases with N ion implantation. The variation in particle sizes for P film and N ion implanted CeO_2 thin films obtained from AFM are found to be consistent with the crystallite sizes of XRD (see in Table 1).

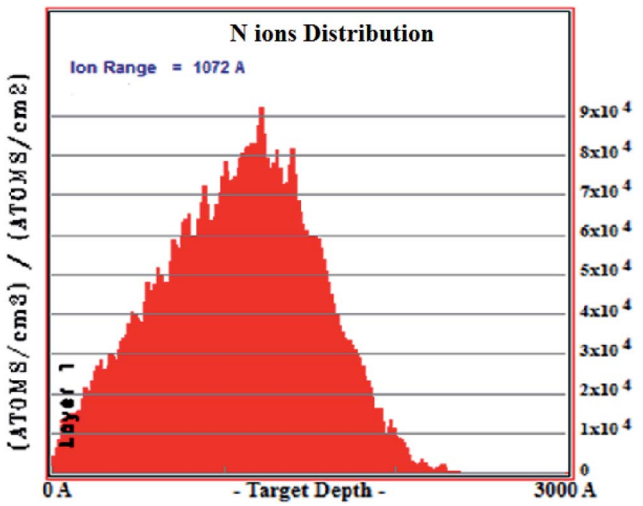

Fig. 4 Depth distribution of 80 keV N ions in CeO_2 thin film.

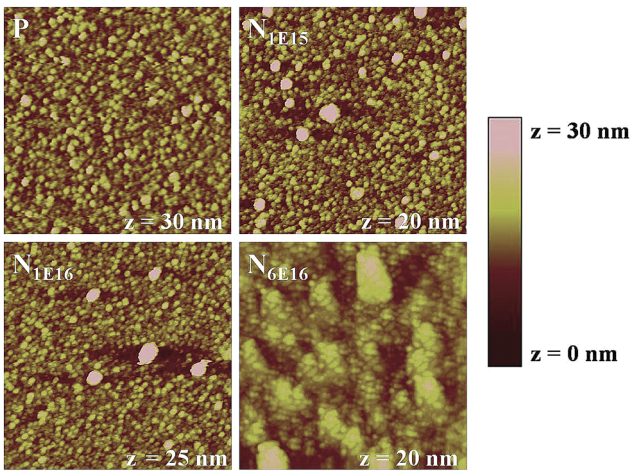

Fig. 5 AFM images (size: 2 × 2 μm^2) of P and N ion implanted CeO_2 thin films.

3.4 Raman spectroscopy

Raman spectroscopy provides the structural and additional details like defects created in the materials. Fig. 6 shows the Raman spectra of all the thin films investigated in this study. The prominent peak at ~443 to 463 cm^{-1} is ascribed to Raman-active vibrational mode (F_{2g}) of CeO_2, which arises due to symmetrical stretching mode of O anions around Ce cations (O–Ce–O).[33] The Raman spectra of implanted films show small shift in F_{2g} mode towards higher wavelength and broadening in FWHM with ion fluence. Presence of inhomogeneous strain and defects contribute to the structural changes in the Raman spectra.[34] It is also evident that the intensity of F_{2g} mode enhances upto N_{1E16} ion fluence and the intensity decreases for N_{6E16} film. Besides, the prominent peak (F_{2g}) mode in N ion implanted CeO_2 thin films show additional peaks at about 620 cm^{-1} and 670 cm^{-1}. The peak positioned at ~620 cm^{-1} is attributed to intrinsic V_O that arise to the reduction of Ce^{4+} to Ce^{3+} ions. This indicates that O sublattice is affected as a result of change in grain size and doping.[35] However, the peak appears at around 670 cm^{-1} might be attributed to second-order Raman transition of CeO_2.[36] Further, the intensity of intrinsic V_O mode at about 620 cm^{-1} and second-order Raman transition about 670 cm^{-1} in CeO_2 films suppresses for higher N ion fluences (*i.e.*, N_{1E16} and N_{6E16}).

3.5 UV-visible analysis

To determine the band gap energies of P and N ion implanted thin films, the Kubelka–Munk (KM) equation was employed which is given as,[26]

$$\frac{K}{S} = \frac{(1 - R_\infty)^2}{2R_\infty} = F(R_\infty) \quad (3)$$

where K, S, R_∞ and $F(R_\infty)$ are known as KM absorption coefficient, KM scattering coefficient, $R_\infty = R_{sample}/R_{standard}$ and KM function respectively. The direct band gap of the semiconductor can be evaluated using the following equation,[37]

$$\alpha h\nu = C_1(h\nu - E_g) \quad (4)$$

where, α is so called linear absorption coefficient of the material, C_1 is a constant of proportionality and $h\nu$ corresponds to photon energy. Using the KM function in eqn (4) following expression can be obtained,

$$[F(R_\infty)h\nu]^2 = C_2(h\nu - E_g)^{1/2} \quad (5)$$

Therefore, computing $F(R_\infty)$ from eqn (3) and plotting $[F(R_\infty)h\nu]^2$ *vs.* $h\nu$, the band gap (E_g) of a films can be obtained.[33] Fig. 7 displays the UV-vis reflectance spectra of P film and N_{1E15}, N_{1E16} and N_{6E16} thin films. The optical band gap of P film is found to be 3.22 eV which is consistent with literature.[38] It is observed that the band gap initially increases for N_{1E15} film (3.43 eV) and then it decreases for higher fluences N_{1E16} (3.22 eV) and N_{6E16} (2.98 eV). The variations in band gap for N ion implanted CeO_2 are found to be consistent with XRD results. As discussed in XRD section, the N occupies interstitial site for N_{1E16} and N_{6E16} films compared with substitutional site for N_{1E15} film. Thus, the non-uniform distribution of N into CeO_2 lattice for lower and higher fluences might be the reason behind the inconsistent change in band gap. This is also consistent with XRD and Raman data. It is believed that different kinds of defects are produced during N ion implantation. Similar results were reported by Xue *et al.* in optical band gaps after N ion implantation.[39]

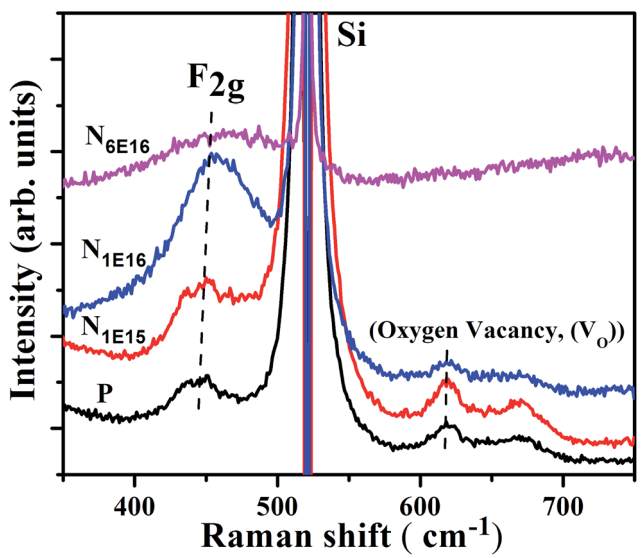

Fig. 6 Raman spectra of P and N ion implanted CeO_2 thin films.

3.6 Photoluminescence studies

The room-temperature PL spectra of the P and N ion implanted CeO_2 thin films measured using 280 nm excitation wavelength are shown in Fig. 8. The PL spectra exhibit wide emission band ~395 nm (~3.13 eV) for P film and sharp emission bands for N ion implanted films ~370 nm. The strong UV emission for P and N_{1E15}, N_{1E16} and N_{6E16} films indicate that optical band gap changes with N ion implantation. Based on this PL study, the emission bands lying between 365–400 nm for CeO_2 thin films are ascribed to the charge transfer from Ce 4f to O 2p band due to different defect levels.[40,41] The weak bands at 400, 460 and 470 nm are found for N ion implanted films. The observed band gap results are consistent with UV-vis spectroscopic results. It is suggested that the strong emission ~369 nm for CeO_2 is attributed to the defects like dislocations or O defects supporting for prompt O mobility.[40,41]

3.7 Magnetic measurements

Fig. 9 shows the magnetization (M) *vs.* applied magnetic field (H) dependence for P and N ion implanted CeO_2 thin films. Inset in Fig. 9 displays the coercivity of P film and N ion implanted CeO_2 thin films. It is evident that the values of saturation magnetization and coercivity are higher for N ion implanted films compared with P. Usually, pure CeO_2 exhibits diamagnetic behaviour.[42] However, the presence of defects such as V_O charge imbalance and the nanosized effects are possible

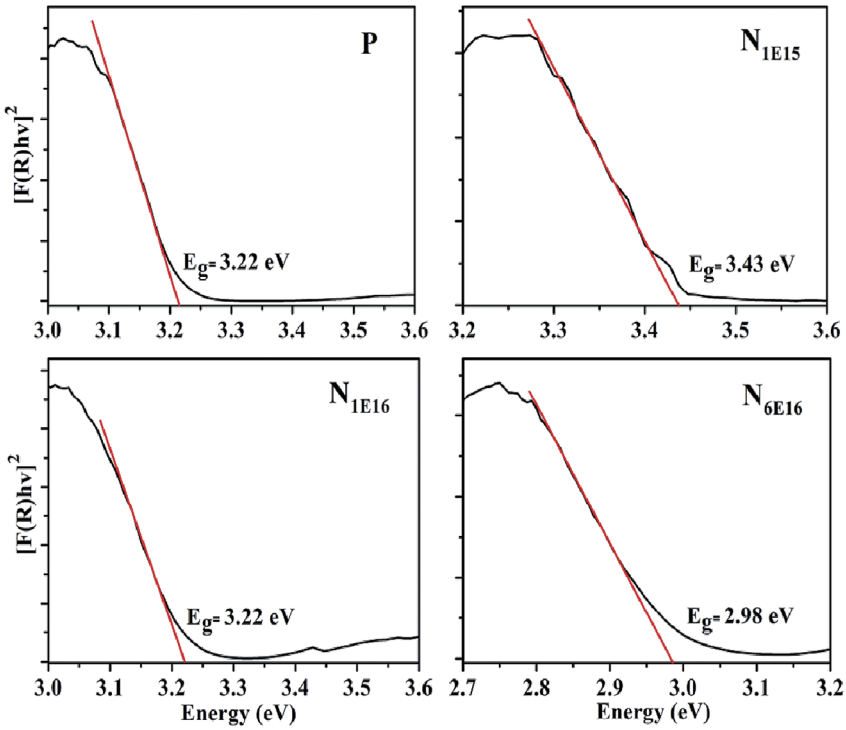

Fig. 7 UV-vis reflectance of P and N ion implanted CeO_2 thin films.

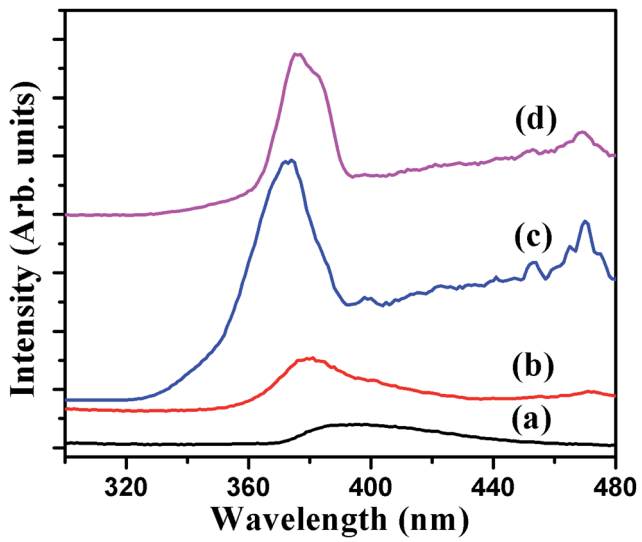

Fig. 8 Room-temperature PL spectra of P and N ion implanted CeO_2 thin films: (a) P, (b) N_{1E15}, (c) N_{1E16}, and (d) N_{6E16}.

causes for FM in CeO_2.[43] It was proposed by Novica *et al.* that surface of nanoparticles plays a crucial role in RTFM which is an intrinsic property of nanocrystalline CeO_2.[42] The experimental and theoretical reports suggest that V_O plays an important role in establishing FM in nanosized CeO_2 and there exist a strong correlation between V_O and the saturation magnetization.[44,45] Ge *et al.* proposed that spin polarization of 4f-shell electrons of Ce ions around V_O cause net magnetic moment for pure CeO_2.[45] It is accepted that the F-center exchange mechanism is suitable to explain the ferromagnetic ordering in nanosized CeO_2.[46] In accordance to this, V_O (F-center) traps an electron which acts as a coupling agent between magnetic Ce^{3+} ions resulting in the formation of overlapped magnetic polarons. There are three possible charge states for the V_O: (a) when no electron is trapped in V_O, called F^{2+} center, (b) when one electron is trapped in V_O which can mediate ferromagnetic ordering known as F^+ center, and (c) when two electrons are trapped in V_O and show singlet ($S = 0$) state which mediates weak antiferromagnetic ordering known as F^0 center.[47,48] It is predicted from theoretical

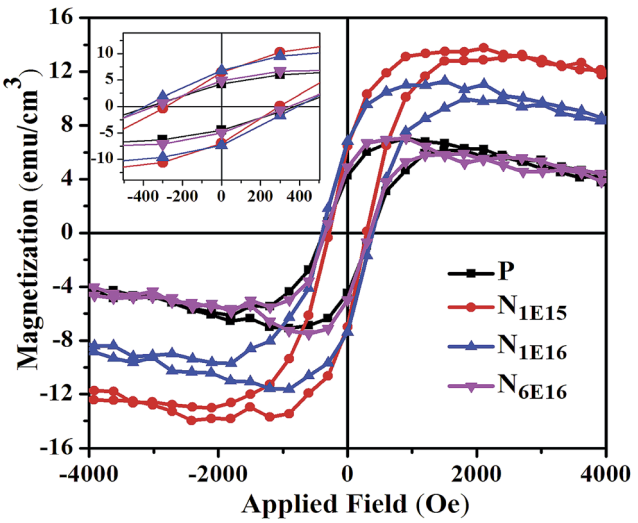

Fig. 9 Room temperature $M - H$ plot of P film and N ion implanted CeO_2 thin films.

calculation that V_O moves from nanoparticles interior to surface.[49] Previous reports suggest that surface layers play a significant role in the establishment of FM compared with interior of sample.[50] The substitution of N impurities near the vacancies may lead to form defect complexes which strongly affect the RTFM in MgO samples.[24] It is clearly seen from the Fig. 9 that P and N ion implanted films show hysteresis loops which indicate RTFM in CeO_2 films. The observed RTFM for pristine CeO_2 film might be recognized due to the presence of V_O. It is established from the XRD results that N occupies the O site in the host CeO_2 lattice. The inclusion of trivalent N ion at divalent O site generates excess charges which are compensated through the introduction of V_O. Therefore, the incorporation of N ion (N_{1E15}) into the host CeO_2 lattice gives rise to increase in saturation magnetization up to a particular N concentration. This increase in V_O or O-related defects might be responsible for enhancement of saturation magnetisation in the N_{1E15} film. However, at higher fluence (*i.e.* N_{1E16} and N_{6E16}), the N ions are distributed non-uniformly and occupy some interstitial sites as confirmed by XRD measurement. Incorporation of N ions at interstitial sites results in the suppression of magnetic moment and hence reduction in RTFM. The decrease in saturation magnetization with further increase in N ion fluence is correlated with decreasing V_O. The increasing V_O or defects at low fluence (N_{1E15}) and decreasing V_O with further increase in N ion fluence compared with P is clearly evident from the Raman spectra (see Fig. 6). These observed results are in well agreement with C implanted ZnO thin films.[15]

Based on density functional theory (DFT) calculations, Valentin *et al.* suggested that N doping in anatase TiO_2 reduces the energy required for the formation of V_O in bulk form.[51] It is easy to reduce the pure rutile TiO_2 than anatase TiO_2. This phase also favours the presence of substitutional N.[52] Furthermore, it is reported that in case of rutile phase, the energy required for the formation of vacancy reduces from 4.3 to 1.0 eV whereas for substitution of O with N from 9.7 to 6.4 eV.[51] As 2p orbital of N^{2-} occupies one electron less than O, the binding energy of the 2p bonding electrons is lower compared with the O ion.[14] In this way, the one electron state of N^{2-} ion will have larger orbital radius as compared to an isolated ion. At a suitable N concentration, the corresponding orbitals of the nearest defects will overlap, giving rise to a narrow impurity band with one hole per N ion leading to magnetic moment. For the two holes in 2p orbitals of O or N ions have lowest configurations that exhibit spin triplet state corresponding to the existence of an associated magnetic moment.[14] The overlapping between the defect states and the formation of a defect band may result in magnetic clusters and hence lead to induce RTFM in N ion implanted CeO_2 thin films. The interstitial occurrence of N ions suppresses the magnetic moments which result in the reduction of RTFM. The effect of C dopant on the magnetic properties of ZnO thin films has been studied theoretically as well as experimentally.[15] Pan *et al.* proposed experimentally as well as based on theoretical calculations (DFT) that the saturation magnetization increases for low carbon concentrations (from 0 to 1 at%). However, it decreases when C concentration reaches about 5 at% in the sample.[53] Zhou *et al.* also investigated experimentally the effect of C concentration (at%) over magnetization and showed that the saturation magnetization is highest at C concentration ~2 at% whereas it reduced with higher concentration of C.[54] It has been suggested that the non-uniform distribution of C atoms at higher concentrations may be the reason. Based on theoretical studies, Ye *et al.* reported that the increase in the C content results in decrease in the separation among C–C ions favouring dominance of antiferromagnetic in the host lattice over the FM nature at higher concentration.[55] Based on these results, it is interpreted that strength of the exchange coupling is directly correlated with the separation between the C–C atoms. On the basis of above findings, in the present case the N ions are distributed non-uniformly inside host CeO_2 lattice at higher N fluences (N_{1E16} and N_{6E16}). This is consistent with the findings of Kumar *et al.*[15] We have also observed that the maximum saturation magnetization is achieved at lower N concentration *i.e.*, 0.14% and decreases for the higher N ion concentrations (1.4% and 8.4%). In context of these calculations and observed experimental results, it is realized that the distribution of N inside the host CeO_2 lattice plays a significant role to modify the magnetic properties. The modification in the magnetic properties by N ion implantation provides an evidence for creating DMO material based spintronics.

4. Conclusions

The structural, morphological, optical and magnetic properties of N implanted CeO_2 thin films were investigated. The XRD confirmed the FCC structure corresponding to CeO_2, and the Raman results show the presence of defects such as oxygen vacancies in these thin films. The band gap of CeO_2 film was found to be ~3.22 eV which is consistent with previous reports. RBS measurement confirms the presence of N ions in the CeO_2 films. The RTFM was observed in the pristine CeO_2 and an enhancement in saturation magnetization and residual magnetization for low fluence N ion implanted CeO_2 thin film. These changes are attributed to the creation of V_O due to N replacing O in CeO_2 lattice. A possible mechanism, the F-center exchange mechanism, is discussed to understand the FM ordering in these films. It is proposed that the distribution of N ions inside the host CeO_2 lattice plays a significant role to modify the magnetic properties.

Acknowledgements

One of the authors, Pawan Kumar, is thankful to the CSIR, New Delhi for providing the SRF fellowship. He also gratefully acknowledges the support and encouragement received from Inter University Accelerator Centre, New Delhi, India.

References

1 P. Singh, K. M. K. Srivatsa and S. Das, *Adv. Mater. Lett.*, 2015, **6**, 371–376.
2 A. Thurber, K. M. Reddy, V. Shutthanandan, M. H. Engelhard, C. Wang, J. Hays and A. Punnoose, *Phys. Rev. B: Condens. Matter Mater. Phys.*, 2007, **76**, 165206.

3 A. Sharma, M. Varshney, H. J. Shin, Y. J. Park, M. G. Kim, T. K. Ha, K. H. Chae and S. Gautam, *Phys. Chem. Chem. Phys.*, 2014, **16**, 19909.
4 M. Venkatesan, C. B. Fitzgerald and J. M. D. Coey, *Nature*, 2004, **430**, 630.
5 N. H. Hong, J. Sakai, N. Poirot and V. Brize, *Phys. Rev. B: Condens. Matter Mater. Phys.*, 2006, **73**, 132404.
6 M. I. B. Bernardi, A. Mesquita, F. Béron, K. R. Pirota, A. O. de Zevallos, A. C. Doriguettod and H. B. de Carvalho, *Phys. Chem. Chem. Phys.*, 2015, **17**, 3072–3080.
7 J. C. Bear, P. D. McNaughter, P. Southern, P. O'Brien and C. W. Dunnill, *Crystals*, 2015, **5**, 312–326.
8 T. Dietl, H. Ohno, F. Matsukura, J. Cibert and D. Ferrand, *Science*, 2000, **287**, 1019–1022.
9 X. P. Han, J. Lee and H. I. Yoo, *Phys. Rev. B: Condens. Matter Mater. Phys.*, 2009, **79**, 100403.
10 M. Y. Ge, H. Wang, E. Z. Liu, J. F. Liu, J. Z. Jiang, Y. K. Li, Z. A. Xu and H. Y. Li, *Appl. Phys. Lett.*, 2008, **93**, 062505.
11 J. M. D. Coey, A. P. Douvalis, C. B. Fitzgerald and M. Vankatesan, *Appl. Phys. Lett.*, 2004, **84**, 1332–1334.
12 Y. L. Liu, Z. Lockman, A. Aziz and J. MacManus-Driscoll, *J. Phys.: Condens. Matter*, 2008, **20**, 165201.
13 K. S. Ranjith, P. Saravanan, S. H. Chen, C. L. Dong, C. L. Chen, S. Y. Chen, K. Asokan and R. T. Rajendrakumar, *J. Phys. Chem. C*, 2014, **118**, 27039–27047.
14 M. M. Cruz, R. C. da Silva, N. Franco and M. Godinho, *J. Phys.: Condens. Matter*, 2009, **21**, 206002.
15 P. Kumar, H. Malik and K. Asokan, *EPL*, 2015, **110**, 67006.
16 H. Pan, J. B. Yi, L. Shen, R. Q. Wu, J. H. Yang, J. Y. Lin, Y. P. Feng, J. Ding, L. H. Van and J. H. Yin, *Phys. Rev. Lett.*, 2007, **99**, 127201.
17 I. S. Elfimov, A. Rusydi, S. I. Csiszar, Z. Hu, H. H. Hsieh, H. J. Lin, C. T. Chen, R. Liang and G. A. Sawatzky, *Phys. Rev. Lett.*, 2007, **98**, 137202.
18 P. Kumar, V. Sharma, A. Sarwa, A. Kumar, S. Surbhi, R. Goyal, K. Sachdev, S. Annapoorni, K. Asokan and D. Kanjilal, *RSC Adv.*, 2016, **6**, 89242.
19 H. Pan, J. B. Yi, L. Shen, R. Q. Wu, J. H. Yang, J. Y. Lin, Y. P. Feng, J. Ding, L. H. Van and J. H. Yin, *Phys. Rev. Lett.*, 2007, **99**, 127201.
20 L. C. Ming, G. H. Quan, X. Xia, Z. Yan, J. Yong, C. Men and Z. X. Tao, *Chin. Phys. B*, 2011, **20**, 047505.
21 G. D. Liu, S. L. Ji, L. L. Yin, G. T. Fei and C. H. Ye, *J. Phys.: Condens. Matter*, 2010, **22**, 046002.
22 M. Kapilashrami, J. Xu, K. V. Rao, L. Belova, E. Carlegrim and M. Fahlman, *J. Phys.: Condens. Matter*, 2010, **22**, 345004.
23 B. M. Maoz, E. Tirosh, M. B. Sadan and G. Markovich, *Phys. Rev. B: Condens. Matter Mater. Phys.*, 2011, **83**, 161201.
24 Q. Li, B. Ye, Y. Hao, J. Liu, W. Kong and B. Ye, *Nucl. Instrum. Methods Phys. Res., Sect. B*, 2013, **297**, 29–34.
25 S. Zhou, Q. Xu, K. Potzger, G. Talut, R. Grötzschel, J. Fassbender, M. Vinnichenko, J. Grenzer, M. Helm, H. Hochmuth, M. Lorenz, M. Grundmann and H. Schmidt, *Appl. Phys. Lett.*, 2008, **93**, 232507.
26 R. Kumari, A. Sahai and N. Goswami, *Prog. Nat. Sci.: Mater. Int.*, 2015, **25**, 300–309.
27 L. Yiwei, Z. Qingfeng and L. Run-Wei, *Chin. Phys. B*, 2013, **22**, 127502.
28 B. Cord, W. Maass, J. Schroeder, K.-H. Schuller and U. Patz, *Thin Solid Films*, 1989, **175**, 287–293.
29 P. Kumar, P. Kumar, A. Kumar, R. C. Meena, R. Tomar, F. Chand and K. Asokan, *J. Alloys Compd.*, 2016, **672**, 543–548.
30 D. P. Padiyan, A. Marikani and K. R. Murali, *Mater. Chem. Phys.*, 2003, **78**, 51.
31 R. K. Hailstone, A. G. DiFrancesco, J. G. Leong, T. D. Allston and K. J. Reed, *J. Phys. Chem. C*, 2009, **113**, 15155–15159.
32 R. Abaira, T. Dammak, A. Matoussi and A. Younes, *Superlattices Microstruct.*, 2016, **91**, 365–374.
33 P. C. A. Brito, D. A. A. Santos, J. G. S. Duque and M. A. M. Macedo, *Phys. B*, 2010, **405**, 1821–1825.
34 Z. V. Popovic, Z. D. Mitrovic, M. Scepanovic, M. G. C. Brojcin and S. Askrabic, *Ann. Phys.*, 2011, **523**, 62–74.
35 S. Phokha, S. Pinitsoontorn and S. Maensiri, *Nano-Micro Lett.*, 2013, **5**, 223–233.
36 S. Dogra, N. D. Sharma, J. Singh, H. K. Poswal, S. M. Sharma and A. K. Bandyopadhyay, *High Press. Res.*, 2011, **31**, 292–303.
37 J. I. Pankove, *Optical Processes in Semiconductors*, Courier Corporation, 2012.
38 S. A. Ansari, M. M. Khan, M. O. Ansari, S. Kalathil, J. Lee and M. H. Cho, *RSC Adv.*, 2014, **4**, 16782.
39 S. W. Xue, L. X. Shao and J. Zhang, *Journal of Optoelectronic and Biomedical Materials*, 2009, **1**, 34–41.
40 P. Goel, M. Arora and A. M. Biradar, *RSC Adv.*, 2014, **4**, 11351.
41 G. Wang, Q. Mu, T. Chen and Y. Wang, *J. Alloys Compd.*, 2010, **493**, 202–207.
42 N. Paunovi, Z. D. Mitrovi, R. Scurtu, S. Askrabic, M. Prekajski, B. Matovic and Z. V. Popovic, *Nanoscale*, 2012, **4**, 5469.
43 M. Varshney, A. Sharma and H. J. Shin, *Adv. Sci., Eng. Med.*, 2015, **15**, 1–7.
44 A. Sundaresan and C. N. R. Rao, *Nano Today*, 2009, **4**, 96–106.
45 V. Fernandes, P. Schio, A. J. A. deOliveira, W. A. Ortiz, P. Fichtner, L. Amaral, I. L. Graff, J. Varalda, N. Mattoso, W. H. Schreiner and D. H. Mosca, *J. Phys.: Condens. Matter*, 2010, **22**, 216004.
46 R. K. Singhal, P. Kumari, A. Samariya, S. Kumar, S. C. Sharma, Y. T. Xing and E. B. Saitovitch, *Appl. Phys. Lett.*, 2010, **97**, 172503.
47 L. R. Shah, A. Bakhtyar, Z. Hao, W. G. Wang, Y. Q. Song, H. W. Zhang, S. I. Shah and J. Q. Xiao, *J. Phys.: Condens. Matter*, 2009, **21**, 486004.
48 J. M. D. Coey, M. Venkatesan and C. B. Fitzgerald, *Nat. Mater.*, 2005, **4**, 173–179.
49 J. C. Conesa, *Surf. Sci.*, 1995, **339**, 337–352.
50 X. Chen, L. Guangshe, S. Yiguo, Q. Xiaoqing, L. Liping and Z. Zhigang, *Nanotechnology*, 2009, **20**, 115606.
51 C. D. Valentin, G. Pacchioni, A. Selloni, S. Livraghi and E. Giamello, *J. Phys. Chem. B*, 2005, **109**, 11414.
52 A. Bouzoubaa, A. Markovits, M. Calatayud and C. Minot, *Surf. Sci.*, 2005, **583**, 107.

53 H. Pan, J. B. Yi, L. Shen, R. Q. Wu, J. H. Yang, J. Y. Lin, Y. P. Feng, J. Ding, L. H. Van and J. H. Yin, *Phys. Rev. Lett.*, 2007, **99**, 127201.
54 S. Zhou, Q. Xu, K. Potzger, G. Talut, R. Grotzschel, J. Fassbender, M. Vinnichenko, J. Grenzer, M. Helm, H. Hochmuth, M. Lorenz, M. Grundmann and H. Schmidt, *Appl. Phys. Lett.*, 2008, **93**, 232507.
55 X. J. Ye, C. S. Liu, W. Zhong, H. A. Song, C. T. Au and Y. W. Du, *Phys. Lett. A*, 2010, **374**, 496.